55/52Mn2+ Complexes with a Bispidine-Phosphonate Ligand: High Kinetic Inertness for Imaging Applications

Maryame Sy, Daouda Ndiaye, Isidro da Silva, Sara Lacerda, Loïc J. Charbonnière, Éva Tóth, Aline M. Nonat

$^{55/52}Mn^{2+}$ complexes with a bispidine-phosphonate ligand: high kinetic inertness for imaging applications

Maryame Sy,[a‡] Daouda Ndiaye,[b‡] Isidro da Silva,[c] Sara Lacerda,[b] Loïc J. Charbonnière,[a] Éva Tóth,[b*] Aline M. Nonat,[a*]*

[a] Equipe de Synthèse pour l'Analyse, Université de Strasbourg, CNRS, IPHC UMR 7178, F-67 037 Strasbourg, France. Email : l.charbonn@unistra.fr; aline.nonat@unistra.fr

[b] Centre de Biophysique Moléculaire, CNRS UPR 4301, Université d'Orléans, rue Charles Sadron, F-45071 Orléans, France. Email : eva.jakabtoth@cnrs-orleans.fr

[c] CEMHTI, CNRS UPR3079, Université d'Orléans, F-45071 Orléans 2, France.

‡ These authors have contributed equally to this work.

KEYWORDS : manganese / ^{52}Mn / kinetic inertness / bispidine / aminophosphonate / MRI / contrast agent / radiolabelling / PET

ABSTRACT

Bispidine (3,7-diazabicyclo[3.3.1]nonane) provides a rigid and preorganized scaffold which is particularly interesting for the stable and inert complexation of metal ions, especially for their application in medical imaging. In this study, we present the synthesis of two bispidine ligands with *N*-methanephosphonate ($H_4\mathbf{L^1}$) and *N*-methanecarboxylate ($H_3\mathbf{L^2}$) substituents as well as the physico-chemical properties of the corresponding Mn^{2+} and Zn^{2+} complexes. The two complexes $[Mn(\mathbf{L^1})]^{2-}$ and $[Mn(\mathbf{L^2})]^{-}$ have relatively moderate thermodynamic stability constants according to potentiometric titrations data. However, they both display an exceptional kinetic inertness, as assessed by transmetallation experiments in the presence of 50 equiv. excess of Zn^{2+}, showing only ~40% and 20% of dissociation for $[Mn(\mathbf{L^1})]^{2-}$ and $[Mn(\mathbf{L^2})]^{-}$, respectively, after 150 days at pH 6 and 37 °C. Proton relaxivities amount to r_1 = 4.31 $mM^{-1}s^{-1}$ ($[Mn(\mathbf{L^1})]^{2-}$) and 3.64 $mM^{-1}s^{-1}$ ($[Mn(\mathbf{L^2})]^{-}$) at 20 MHz, 25 °C, and are remarkable for Mn^{2+} complexes with one inner-sphere water molecule (q = 1); they are comparable to that of the commercial contrast agent $[Gd(DOTA)(H_2O)]^{-}$. The presence of one inner-sphere water molecule and an associative water exchange mechanism were confirmed by temperature-dependent transverse ^{17}O relaxation rate measurements, which yielded $k_{ex}^{298} = 0.12\times10^7$ s^{-1} and 5.5×10^7 s^{-1} for the water exchange rate of the phosphonate and the carboxylate complex, respectively. In addition, radiolabelling experiments with ^{52}Mn were also performed with $H_2(\mathbf{L^1})^{2-}$ showing excellent radiolabelling properties and quantitative complexation at pH 7 in 15 min at room temperature, as well as excellent stability of the complex in various biological media over 24h.

Introduction

The search for thermodynamically stable and kinetically inert manganese(II) complexes is a challenging and topical subject with high potential impact for the field of medical imaging. Indeed, Mn^{2+}-chelates have emerged as safer and more biocompatible alternatives to current Gd-based Magnetic Resonance Imaging (MRI) contrast agents, whose safety has recently been questioned in relation to the potential *in vivo* release of free and toxic Gd^{3+}. The causal link of nephrogenic systemic fibrosis to Gd^{3+} exposure of patients[1] has so far led to the withdrawal of Gd^{3+} complexes formed with linear chelators. Nevertheless, brain and bone accumulation of gadolinium remains a risk, even for highly stable and inert macrocyclic derivatives such as GdDOTA.[2] Manganese is an essential endogeneous trace element that

contributes to the assimilation of lipids, proteins and carbohydrates by our body and has a role in normal energy metabolism.[3] When associated with superoxide dismutase, manganese helps protect cells against oxidative stress. It also contributes to the normal formation of connective tissues. Manganese also plays a role in the growth and maintenance of bones, which are therefore the main organs for receiving Mn in the body.[4] As an order of magnitude, the World Health Organization (WHO) reports that the Reference Man contains about 12 mg Mn in the entire body (10 to 20 mg), with an average of 45% stored in bones.[5] The remaining circulating Mn (6.6 mg, 24 μM in average) has a very short half-life in blood due to the homeostatic control of Mn by absorption in the body and liver excretion.[6] With respect to MRI contrast agent application, Mn^{2+} possesses favorable electronic properties (S = 5/2, slow electron spin relaxation with T_{1e} values ideally on the nanosecond scale)[7] in order to efficiently enhance the nuclear relaxation of water protons. Finally, ^{52}Mn is an emerging positron emitting radionuclide with suitable energy (E_{max} = 0.6MeV), half-life ($t_{1/2}$ = 5.6 days) and branching ratio (29%) for application in Positron Emission Tomography (PET) with high resolution.[8] The long half-life value of positron decay is advantageous for target separation and chemical handling of the radionuclide, and particularly interesting for the PET investigation of slow biological processes, *e.g.* the pharmacokinetics of long circulating proteins like antibodies. Such studies are for the moment limited to animal studies due to the relatively high radiation. In overall, manganese is the only element that offers combined detection capabilities in MRI and PET.[9-10]

The search for safer MRI contrast agent alternatives and the rapid development of bimodal imaging combining PET and MRI have created a strong need for new Mn^{2+} chelators that satisfy requirements for both PET (using an infinitesimal quantity of ^{52}Mn) and MR imaging (using the natural isotope ^{55}Mn). These requirements involve high thermodynamic stability and kinetic inertness of the complex, and good relaxation efficacy for MRI. A major challenge in the design of appropriate ligands arises from the lack of ligand-field stabilization for Mn^{2+} complexes in the high-spin d^5 electronic configuration, which makes them inherently less stable than their other transition metal counterparts or than current Gd^{3+}-based MRI agents. Furthermore, to produce a significant proton relaxation enhancement and MRI efficiency, it is important that the chelator ensures good stability without saturating the coordination sphere of Mn^{2+} (typical coordination numbers are 6 and 7), thus maintaining room for at least one inner-sphere water molecule. The optimal exchange rate of this water molecule with bulk is also a parameter to be taken into account in MRI contrast agent development, in particular if the objective is to incorporate the Mn^{2+} complex in

macromolecular constructs; although we should note that Mn^{2+} complexes tend to have rather fast water exchange, which makes this issue less critical.

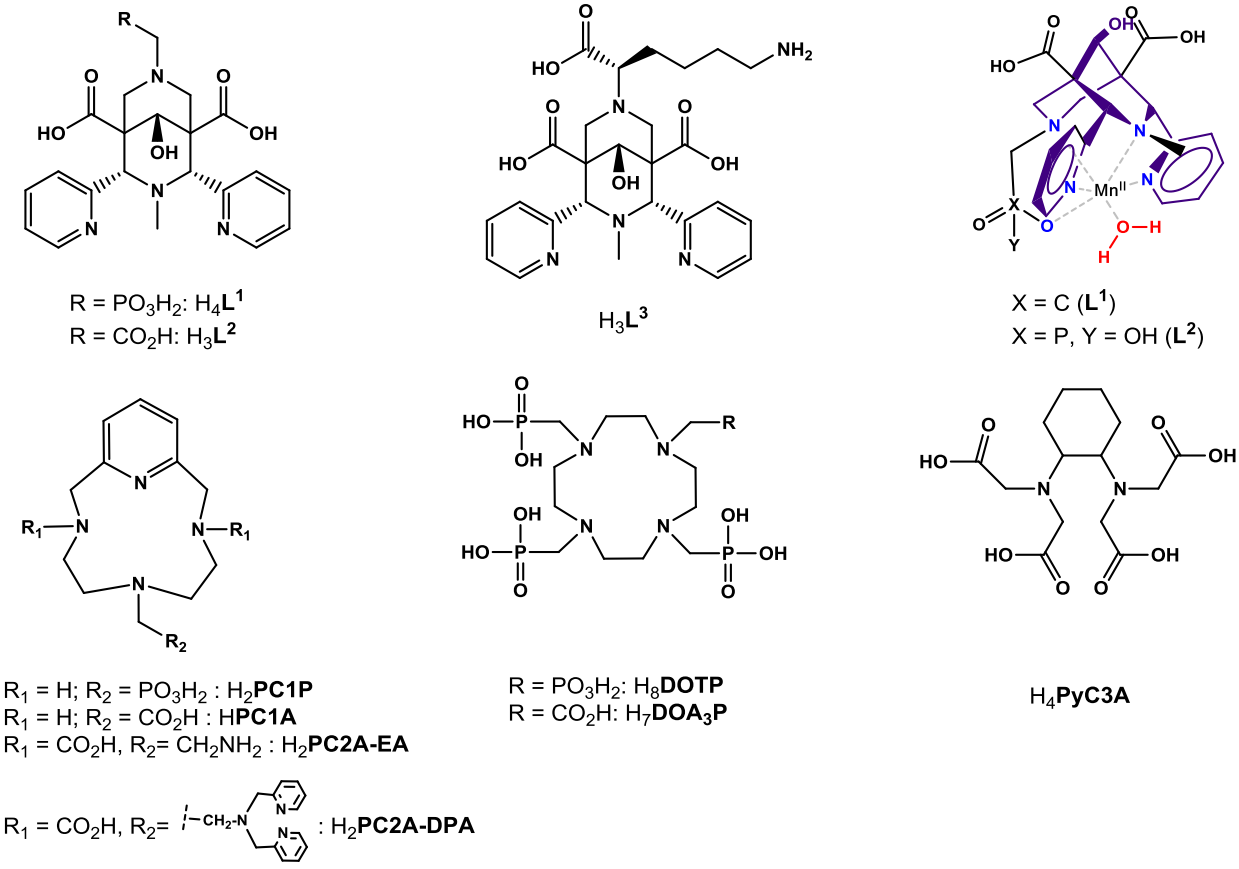

Scheme 1. Ligands discussed and schematic representation of the Mn(II) complexes with $\mathbf{L^1}$ and $\mathbf{L^2}$.

Several recent studies have demonstrated that, as far as medical imaging applications are concerned, high thermodynamic stability of the complex solely is not sufficient for its *in vivo* non-toxicity. Once the contrast agent is injected into the body, the system is not in equilibrium; hence, kinetic inertness of the complex becomes the determining factor to prevent free metal release.[11] Mn^{2+} complexes are typically very labile which sets thus another challenge. Kinetic inertness can be evaluated by monitoring the dissociation of complexes in competitive media, which corresponds usually either to an excess of a competitive cation such as Zn^{2+}, or to an acidic medium. It is important to note that there is no direct correlation between the thermodynamic stability and the kinetic inertness of the complexes; the most thermodynamically stable complexes are not necessarily kinetically inert.

Recent years have witnessed very intensive research to identify Mn^{2+} chelates with sufficient kinetic inertness. Among acyclic ligands, those with a rigidified cyclohexyl-diamine backbone proved to be the best.[12-14] In the family of macrocyclic chelators, pyclen-derivatives, especially those bearing amide coordinating functions gave very interesting

results.[15-17] In the case of amide ligands, their weaker basicity with respect to that of the acetate analogues is responsible for a slower dissociation via the proton-assisted pathway.
The bispidine-type [Mn(H**L**^{3})] complex is particularly interesting in terms of kinetic inertness, since no dissociation could be observed over a period of 130 days at pH 6, 37 °C and in the presence of 50 equiv. of Zn^{2+},[18] while under similar conditions, $[MnH(PC2A\text{-}EA)]^{+}$ for instance, considered as a particularly inert Mn^{2+} chelate, has a dissociation half-life of 54.4 h (see Scheme 1 for structures).[15] This exceptional resistance to dissociation can be likely related to the highly pre-organized and rigid structure of the bispidine skeleton. In addition, [Mn(H**L**^{3})**]** displays one hydration water molecule which, together with an important second sphere relaxation effect, results in high longitudinal relaxivity (r_1 = 4.28 $mM^{-1}s^{-1}$, 25 °C, 20 MHz, pH 7, H_2O). This value is ~15-20 % higher than the relaxivity of most Mn^{2+} complexes with q =1 and very similar to that of the commercial contrast agent $[Gd(DOTA)(H_2O)]^{-}$ (4.74 $mM^{-1}s^{-1}$; H_4DOTA = 1,4,7,10-tetraazacyclododecane-1,4,7,10-tetraacetatic acid).[19] Further, we could also successfully radiolabel H_2(**L**^{3})$^{-}$ with $^{52}MnCl_2$, with a 99% radiochemical yield (H_2O, pH = 7, 70 °C, 1h), and the radiocomplex was found to be stable in various media up to 18 h (> 91%).[18] Overall, these results make ligand H_2(**L**^{3})$^{-}$ a very attractive candidate for Mn^{2+} complexation in the perspective of MRI and PET imaging.

In the present study, our objective was to investigate the influence of substituents at the N7 position (see Scheme 2 for atom numbering) of the bispidine skeleton on the thermodynamic stability and the kinetic inertness of the corresponding Mn^{2+} complexes, as well as on their efficiency as potential MRI contrast agent and PET tracer. More specifically, we have focused on investigating the effect of the methylene phosphonic acid pendant arm (ligand H_4**L**^{1}), which is expected to strongly influence ligand basicity and steric compression around the metal center with subsequent effects on the thermodynamic stability, the formation and dissociation kinetics of the Mn^{2+} complex, and on parameters impacting relaxivity such as second-sphere contribution and water exchange rate.[20] The analogue ligand with a methylene carboxylic acid pendant arm (H_3**L**^{2}) has been also synthesized and studied for direct comparison. The thermodynamic stabilities of the Mn^{2+} complexes formed with the two ligands have been investigated as well as their dissociation kinetics in the presence of Zn^{2+} in varying pH conditions. The relaxation properties of both complexes have been assessed by a combined variable temperature ^{1}H NMRD and ^{17}O NMR study. Finally, radiolabeling of H_4**L**^{1} with ^{52}Mn has been realized and the stability of the ^{52}Mn-complex investigated.

Experimental Section

General procedures. Solvents and starting materials were purchased from Aldrich, Acros and Alfa Aesar and used without further purification, unless stated otherwise. Solvents for high-performance liquid chromatography (HPLC) were HPLC-grade. All aqueous solutions were prepared with Milli-Q water (ρ < 18MΩ). $MnCl_2.4H_2O$ was obtained from Carlo Erba. Chromium powder 99 %, 100 mesh metal basis density = 2.0-3.0g/cm², was obtained from Alfa-Aesar. Ligand H_4L^1 was obtained according to the procedure described previously.[21] Ligand $H_4\mathbf{L^1}$ and dimethyl-1-methyl-4-oxo-2,6-bis(pyridine-2-yl)piperidine-3,5-dicarboxylate were obtained according to previously reported procedures. Although previously synthesized, ligand $H_3\mathbf{L^2}$ has been obtained from a new synthetic pathway involving intermediate 3, whose synthesis has already been reported. [21-23]

IR spectra were recorded on a Perkin Elmer Spectrum One Spectrophotometer as solid samples and only the most significant absorption bands are given in cm^{-1}. ^1H and ^{13}C NMR spectra and 2D COSY, NOESY, HSQC, and HMBC experiments were recorded either on Bruker Avance 400 and Avance 500 spectrometers (in Strasbourg) or on a Bruker Advance III HD Spectrometer using a 5 mm BBFO probe (in Orléans). ^{13}C NMR spectra were measured with ^1H decoupling. All chemical shifts (δ) values are given in parts per million and are referenced to the solvent.[24] Elemental analyses and mass spectrometry analysis were carried out by the Service Commun d'Analyses of the University of Strasbourg.

Synthesis of $H_3\mathbf{L^2}$.

Compound 1 (dimethyl (2R,4S)-7-(2,4-dimethoxybenzyl)-3-methyl-9-oxo-2,4-di(pyridin-2-yl)-3,7-diazabicyclo[3.3.1]nonane-1,5-dicarboxylate). **P_1** (dimethyl-1-methyl-4-oxo-2,6-di(pyridin-2-yl)piperidine-3,5-dicarboxylate, 1750 mg, 4.56 mmol, 1 *equiv.*) is dissolved in THF (40 mL). 2,4-Dimetoxybenzylamine (910 mg, 5.45 mmol, 1.2 *equiv.*) and formaldehyde 37 % (88 µl, 11 mmol, 2.4 eq) are then added successively. The mixture is heated at reflux for 16 hours and the reaction is monitored by TLC (SiO_2, CH_2Cl_2/MeOH 90/10 as eluent). The solvent is removed and the resulting solid is washed with hot MeOH yielding compound **1** as a colourless solid (2.15 g, 83 %). ^1H NMR ($CDCl_3$, 400 MHz): δ 1.91 (s, 3H, H16); 2.46 (d, 2H, H6/8ax, $^4J_{H6axH8ax}$ = 12.0 Hz); 3.05 (d, 2H, H6/8eq, $^4J_{H6eqH8eq}$ = 12.0 Hz); 3.36 (s, 2H, H9); 3.8 (s, 3H, H12/H14); 3.84 (s, 6H, H15); 3.93 (s, 3H, H12/H14); 4.65 (s, 2H, H2 + H4); 6.41 (dd, J_1 = 8.2 Hz, J_2 = 2.5 Hz, 1H, H11); 6.57 (d, J = 2.5 Hz, 1H, H13); 7.02 (d, J = 8.2 Hz, 1H, H10); 7.1 (m, 2H, Hb); 7.46 (td, J_1 = 7.8 Hz, J_2 = 1.9 Hz, 2H, Hc), 7.98 (d, J = 7.8 Hz, 2H, Hd); 8.34 (m, 2H, Ha); $^{13}C\{1H\}$ NMR ($CDCl_3$, 126 MHz): δ 43.22, 52.47, 55.55 (2C), 55.81, 59.06, 62.09, 74.02, 98.78, 103.86, 117.76, 122.83, 123.73,

133.19, 136.15, 148.90, 158.74, 159.35, 160.76, 168.68, 204.09. Mass Spectroscopy (ESI^+/MS): *m/z* = 575.25 $[M + H]^+$ (calc. 575.25).

Compound 3 (dimethyl (2R,4S,9r)-9-hydroxy-3-methyl-2,4-di(pyridin-2-yl)-3,7-diazabicyclo[3.3.1]nonane-1,5-dicarboxylate). In a solution of compound **1** (6.56 g, 11,4 mmol, 1 equiv.) in THF at -78°C, 0.66 equiv. of sodium borohydride (0.28 g, 7.52 mmol) is added in two portions of 0.14 g at 2 hours of interval and the mixture is stirred at -78 °C for 2 hours. At the end, the reaction is quenched with 40 mL of NH_4Cl and the solvent is removed under vacuum. The CH_2Cl_2 is added, salts are filtered and the solvent is removed under vacuum. The crude product **2** is used for the next step without purification and it is dissolved in a mixture of CH_2Cl_2 (15 mL) and TFA (10 mL). The mixture is stirred at reflux for 16 hours. At the end, the solvent is evaporated and the crude product is dissolved in 20 mL of MeOH and stirred at reflux for 2 hours. A white precipitate is obtained, which is then filtered and the solvent is removed under vacuum. Finally, the crude product is purified by FPLC (SiO_2, 100 % CH_2Cl_2 to 80/20 CH_2Cl_2/MeOH) to give compound **3** (1.62 g) with a 33 % yield. ^{1}H NMR (MeOD, 400 MHz): δ 1.53 (s, 3H, H10); 3.60 (s, 6H, H11); 3.60 (d, 2H, H6/8ax, $^4J_{H6axH8ax}$ = 13.4 Hz); 4.31 (d, 2H, H6/8eq, $^4J_{H6eqH8eq}$ = 13.4 Hz); 4.53 (s, 1H, H9); 4.75 (s, 2H, H2/4); 7.35(m, 2H, Hb); 7.54 (d, *J* = 7.6 Hz, 2H, Hd); 7.97 (td, J_1 = 7.6 Hz, J_2 = 1.9 Hz, 2H, Hc); 8.64 (m, 2H, Ha).

Ligand H_3L^2 (2R,4S,9r)-7-(carboxymethyl)-9-hydroxy-3-methyl-2,4-di(pyridin-2-yl)-3,7-diazabicyclo[3.3.1]nonane-1,5-dicarboxylic acid). Potassium carbonate (163 mg, 1.18 mmol, 2.4 equiv.) is suspended in a solution of compound **3** (210 mg, 0.49 mmol, 1 equiv.) in 25 mL of anhydrous acetonitrile under argon. Then, ethyl bromoacetate (66 µl, 0.59 mmol, 1.2 equiv.) is added and the mixture is heated at 80 °C for 16 hours. The reaction is monitored by TLC (SiO_2, CH_2Cl_2/MeOH 90/10 as eluent). At the end, K_2CO_3 is filtered and solvent is removed under vacuum. The product (**4**) is used for the next step without purification. The crude product is dissolved in a mixture of H_2O (10 mL) and THF (5 mL) and lithium hydroxide (59 mg, 2.45 mmol, 5 eq) is added. The solution is stirred for 16 hours at room temperature. At the end, the solvent is evaporated and the crude product is dissolved in a minimum of H_2O and the pH is lowered to 2 with aqueous HCl. The solution is then purified by FPLC (C_{18}, 97/3 H_2O/MeOH to 50/50 H_2O/MeOH) to give **H_3L^2**.HCl (124 mg) with a 51 % yield. ^{1}H NMR (MeOD, 400 MHz): δ 1.82 (s, 3H, H16); 2.17 (d, 2H, H6/8ax, $^4J_{H6axH8ax}$ = 12.4 Hz); 2.82 (d, 2H, H6/8eq, $^4J_{H6eqH8eq}$ = 12.4 Hz); 2.81 (s, 2H, H10); 3.90 (s, 1H, H9); 4.66 (s, 2H, H2/4); 7.23 (m, 2H, Hb); 7.51 (d, *J* = 7.6 Hz, 2H, Hd); 7.67 (td, J_1 = 7.6 Hz, J_2 = 1.9 H_Z, 2H, Hc); 8.65 (m, 2H, Ha); $^{13}C\{1H\}$ NMR (MeOD, 126 MHz): δ 43.08; 56.80; 59.87;

69.93; 74.84; 124.73; 127.53. 127.70; 138.46; 139.41; 150.27; 158.60; 161.6. Elemental Analysis: Calculated for $C_{22}H_{24}N_4O_7$.HCl, C, 53.61, H, 5.11, N, 11.37. Found: C, 54.01, H, 5.33, N, 11.22. Mass Spectrometry: (ESI^-/MS): *m/z* = 455.15 $[M - H]^-$ (calc. 455.16).

Solution preparation. Ligand concentrations were determined by adding an excess of $ZnCl_2$ solution to the ligand solution and titrating the metal excess with standardised Na_2H_2EDTA in urotropine buffer (pH 5.6 –5.8) in the presence of Xylenol Orange as an indicator. EDTA and our ligands form a 1:1 complex with Zn^{2+}, thus the ligand concentration can be calculated from the difference between the total Zn^{2+} quantity and that titrated with Na_2H_2EDTA. The concentrations of metal solutions were determined by complexometric titrations with standardised Na_2H_2EDTA. The Mn^{2+} complexes were prepared by mixing 1 equiv. of ligand (**L**^{1} or **L**^{2}), with 1 equiv. of $MnCl_2$, and the pH was adjusted to 7.4 either with a buffered solution or by adding KOH or HCl to the solution and the samples were heated at 60 °C for 30 min. The absence of free Mn^{2+} was checked by the Xylenol Orange test (pH 5.8, urotropine buffer). The concentration of Mn^{2+} complex samples was checked by ICP-OES (Jobin Yvon ULTIMA2 Spectrometer, measurements done in 5% HNO_3 matrix) and/or bulk magnetic susceptibility (BMS) measurements. To exclude any oxidation of the Mn^{2+} ion, we have recorded UV-Vis spectra of the complexes over time. These spectra remain identical for several days even when the complex solutions are exposed to air or even after bubbling oxygen through the solutions (see Figure S11). [25]

Potentiometric titrations. Carbonate-free 0.1 M NaOH and 0.1 M HCl were prepared by dilution of concentrated solutions from Fisher Chemicals. Potentiometric titrations were performed in 0.15 M aqueous NaCl under nitrogen atmosphere and the temperature was controlled at 25 ± 0.1 °C with a circulating water bath. The p[H] (p[H] = -log[H^+], concentration in molarity) was measured in each titration with a combined pH glass electrode (Metrohm) filled with 3 M KCl. The titrant addition was automated by the use of a 702 SM titrino system (Metrohm). Prior each experiment, the electrode was calibrated as a hydrogen concentration probe by titrating known amounts of HCl with NaOH in 0.1 M electrolyte solution.[26] A plot of potential versus p[H] allows the determination of the electrode standard potential (E°) and the slope factor (f). The GLEE program was used for the glass electrode calibration.[27-28] Continuous potentiometric titrations with 0.1 M *NaOH w*ere conducted on aqueous solutions containing 1.5-1.8 mM of ligand in 0.15 M *N*aCl (V_0 = 5 mL), with 2 minutes waiting time between successive points. The stability of the ligands has been verified by performing a reverse titration, from basic to acidic pH, on a sample that had been titrated first from acidic to basic pH. The two titration curves are overlapping proving full

reversibility and the stability of the ligand. The titrations of the metal complexes were performed with the same ligand solution to which 1 equiv. of the metal cation had been added. To determine the stability constant of $[Mn(\mathbf{L^1})]^{2-}$ and its protonation constants, a manual direct titration was carried out between pH 2 and 6, with 20 mins waiting time between successive points. In the case of $[Mn(\mathbf{L^2})]^{-}$, batch samples (0.5 mL) were prepared between pH = 2.5 and 7.0 at 1:1 Mn:L^2 ratio ($c_{Mn} = c_L$ = 1.5 mM, 0.15 M NaCl. The samples were kept at 25°C until the equilibrium state was reached (1 day at pH = 2.5 and ~2 hours at pH = 6.5). This was verified by monitoring the stabilization of the relaxivity and the pH values in the samples over time. Experimental data were refined using the computer program Hyperquad 2008.[29] All equilibrium constants are concentration quotients rather than activities and are defined as:

$$K_{mlh} = \frac{[M_m L_l H_h]}{[M]^m [L]^l [H]^h}$$

The ionic product of water at 25 °C and 0.15 M ionic strength is pK_w = 13.77.[30] Fixed values were used for pK_w, ligand acidity constants and total concentrations of metal, ligand and acid. All values and errors (one standard deviation) reported are at least the average of two independent experiments.

Dissociation kinetic studies. Kinetic inertness was assessed at 37 °C and in 0.1 M NaCl, via transmetallation studies of the $[Mn(\mathbf{L^1})]^{2-}$ and $[Mn(\mathbf{L^2})]^{-}$ complexes (1 mM) with Zn^{2+} ($ZnCl_2$) at pH = 6 (0.030 M MES buffer), and at pH = 3.1 (0.050 M KH-phthalate buffer), pH = 3.7 and pH = 4.1 (0.03 M dimethyl-piperazine), and pH = 5 (0.030 M N-methylpiperazine), in the presence of 10- or 50-fold excess of Zn^{2+}. The excess of the exchanging metal ion guarantees pseudo-first order conditions. For the duration of the experiments (up to 5 months), the samples were stored in a thermostat at 37 °C and the water proton relaxation rates at 60 MHz were monitored over time using a Bruker Minispec relaxometer. The pH was controlled for each sample at the end of the kinetic measurements to confirm that it remained stable during the experiment. $[Mn(\mathbf{L^1})]^{2-}$ dissociation was also followed at higher acidities (0.01– 1 M), without Zn^{2+} (25 °C, I = 1 M (NaCl + HCl)).The analysis of the experimental data was performed using Visualiseur/Optimiseur running on a MATLAB 8.3.0 (R2014a) platform.

Relaxometric Measurements. Proton NMRD profiles of $[Mn(\mathbf{L^1})]^{2-}$ and $[Mn(\mathbf{L^2})]^{-}$ complexes were recorded in an aqueous solution (c_{MnL} = 1.8 mM and 1.4 mM, respectively; pH = 7.0) on a Stelar SMARTracer Fast Field Cycling relaxometer (0.01-10 MHz) and a Bruker WP80 NMR electromagnet adapted to variable field measurements (20-80 MHz) and

controlled by a SMARTracer PC-NMR console. The temperature was monitored by a VTC91 temperature control unit and maintained by a gas flow. The temperature was determined by previous calibration with a Pt resistance temperature probe. For the measurements in serum, a concentrated aqueous solution of $[Mn(\mathbf{L^1})]^{2-}$ (2.5 mM) was diluted tenfold in human serum (Sigma Aldrich, St. Louis, Missouri, US).

^{17}O NMR studies. Variable temperature ^{17}O transverse (T_2) relaxation times and chemical shifts of aqueous solution of manganese complexes (for $[Mn(\mathbf{L^1})]^{2-}$: c_{MnL} = 4.58 mol/kg, pH = 7.4 ; for $[Mn(\mathbf{L^2})]^{-}$: c_{MnL} = 4.19 mol/kg, pH = 7.0) were measured using a Bruker ARX 400 spectrometer (9.4 T). As stated before, the absence of free metal ion was checked by the Xylenol Orange test and the concentration of Mn^{2+} was checked by the chemical shift measurement of *tert*-butanol induced by the magnetic susceptibility. The samples were sealed in a glass sphere fitted into a 10 mm NMR tube to eliminate magnetic susceptibility corrections to the chemical shifts.[31] To improve sensitivity in ^{17}O NMR, ^{17}O-enriched water (11.10% $H_2{}^{17}O$, Cortecnet) was added to the solutions to yield approximately 1% ^{17}O enrichment. An acidified water solution ($HClO_4$, pH 3) was used as external reference. It was previously shown that an acidified water reference or the diamagnetic Zn^{2+} analogue of the Mn^{2+} complex measured at the same concentration and pH as the paramagnetic sample give identical results.[32] The temperature was varied between 273 and 348 K. The temperature was calculated according to previous calibration with ethylene glycol and methanol.[30] Transverse relaxation times (T_2) were obtained by the Carr-Purcell-Meiboom-Gill spin-echo technique.[33] The technique of the ^{17}O NMR measurements on paramagnetic complexes has been described in details elsewhere.[34] The ^{17}O NMR data have been treated according to the Solomon-Bloembergen-Morgan theory of paramagnetic relaxation[35] using Visualiseur/Optimiseur running on a MATLAB 8.3.0 (R2014a) platform.

^{52}Mn Radiolabelling. ^{52}Mn ($t_{1/2}$ = 5.6 d) was prepared *via* irradiation of chromium target by proton beam (14 MeV) at the CEMHTI cyclotron (Orléans, France). ^{52}Mn is produced from the ^{52}Cr(p,n)^{52}Mn nuclear reaction. Upon purification via anion exchange columns as previously described,[18] ^{52}Mn is recovered as $^{52}MnCl_2$ solution.

Radiolabelling of $H_2(\mathbf{L^1})^-$. For the radiolabelling, the pH of the ^{52}Mn solution was adjusted to 7 with NaOH in the presence of ascorbic acid. $H_2(\mathbf{L^1})$ was added at a $1{:}10^4$ Mn:L molar ratio and the mixture was incubated for 15 min at room temperature or at a $1{:}10^3$ Mn:L molar ratio and the mixture was incubated for 20 min at 70 °C. The radiolabelling reaction was followed

by thin-layer chromatography (silica gel 60 F254 plates, Merck), using 5% (w/v) ammonium acetate in a 1:1 mixture of methanol and water as mobile phase. The TLCs are exposed by impregnation on a multisensitive phosphorscreen (Packard, Perkin Elmer, Meriden, USA) and revealed on a Cyclone Storage phosphor system (Packard, Perkin Elmer, Shelton, USA). In this system, the free ^{52}Mn does not migrate ($R_f = 0 – 0.1$) while the $[^{52}Mn(\mathbf{L^1})]^{2-}$ complex has a R_f of 0.7.

Lipophilicity. Lipophilicity was assessed through the determination of the octanol/saline partition coefficients (log *P* values), by the ‘‘shakeflask’’ method. Briefly, 100 µL of the $[^{52}Mn(\mathbf{L^1})]^{2-}$ radiocomplex was added to a solution containing 1 mL saline (pH 7.4) (obtained from a saturated octanol solution) and 1 mL of octanol, in triplicate. The resulting solutions were vortexed and centrifuged at 3000 rpm for 10 min. Aliquots of 100 µL were removed from the octanol phase and from the water phase and the activity measured in a gamma counter. The lipophilicity was calculated as the average log ratio value of the radioactivity in the organic fraction and the aqueous fraction from the three samples.

In vitro stability of $[^{52}Mn(\mathbf{L^1})]^{2-}$. The stability of the radiocomplex $[^{52}Mn(\mathbf{L^1})]^{2-}$ (pH 7) was studied in presence of different media: water, saline (0.9 % NaCl), PBS (Dubelcco, pH 7.4, without Ca and Mg) and HSA 0.6 mM. For this, 20 µL aliquots of the $[^{52}Mn(\mathbf{L^1})]^{2-}$ were mixed with 200 µL of the medium, the tubes were kept at room temperature and the radiocomplex stability followed by radioTLC (0.3 µL aliquots) at different time points. The studies were performed in duplicates.

Results and discussion

Synthesis

Ligand $H_4\mathbf{L^1}$ was obtained in three steps from (aminomethyl)phosphonic acid and dimethyl-1-methyl-4-oxo-2,6-bis(pyridine-2-yl)piperidine-3,5-dicarboxylate according to the procedure described previously.[21] Although ligand $H_3\mathbf{L^2}$ had already been synthesized previously by using a double-Mannich reaction with glycine and ethyl glycinate,[36-37] a new protocol has been preferred this time which involves the nucleophilic substitution of intermediate 3, whose synthesis has already been reported.[22-23] The synthesis described on Scheme 2 is equivalent in terms of yield to the previous strategy (20 % from $\mathbf{P_1}$), but has the advantage of increased versatility. Interestingly, reduction of bispidone 2 by sodium borohydride lead to a mixture of two diastereoisomers, which could, for the first time, be separated from

chromatography column on silica (CH_2Cl_2/MeOH eluent). The major diastereoisomer was used for the subsequent steps. Correlation between H9 and axials H6/8 were observed in ^{1}H-^{1}H NOESY experiment indicating that the alcohol function is pointing towards N-CH_3 (Figure S1). For the other diastereoisomers, which was left aside for this study, correlations were seen between H9 and protons H2 and H4 (Figure S2). In this synthesis, intermediate 4 was not isolated but purified only after saponification of the methyl esters with LiOH. This saponification renders the purification by reverse phase chromatographic column (on C18) possible and, according to our observations, avoids product losses. Ligand $H_3\mathbf{L}^2$ was isolated as a hydrochloride salt and the cis configuration of the bispidine skeleton was confirmed from ^{1}H NMR spectrum. In addition, the ^{1}H-^{1}H NOESY spectra indicated that intermediate 3 and following compounds were obtained as a single diastereoisomers with H9 pointing towards NH.

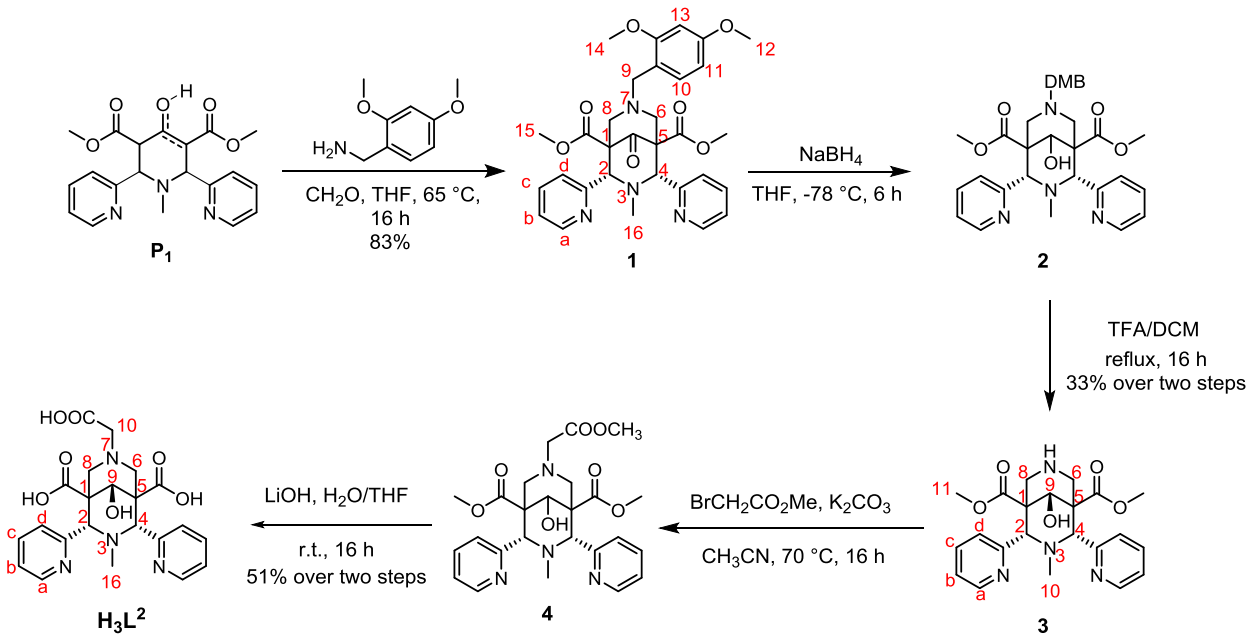

Scheme 2. Synthesis of ligand $H_3\mathbf{L}^2$.

Protonation constants of the ligands and thermodynamic stability constants of the metal complexes

The complexation properties of the ligands depend on their basicity, and the calculation of the thermodynamic stability constants requires ligand protonation constants. The analysis of the pH-potentiometric titration curves (Figure S3) of the ligands yielded four and three logK_H values respectively for $H_4\mathbf{L}^1$ and $H_3\mathbf{L}^2$ (Table 1). For both ligands, a single

protonation constant is observed in the basic pH region, corresponding to the protonation of one of the two tertiary amines of the bispidine bicycle. Previous studies have shown that the protonation degree of the bicycle is intrinsically related to its conformation.[38] In general, depending on the nature and the size of the substituents, the bispidine bicycle can adopt different conformations : chair-chair, chair-boat and boat-boat; among these, the chair-chair conformation is best adapted for metal coordination.[36, 39] In this conformer, only one of the two amines can be protonated in the bicycle which stabilizes this form of the ligand *via* strong hydrogen bonding with the second amine nitrogen. In contrast, diprotonation is always associated with the chair-boat or boat-boat conformations, due to electrostatic repulsion between the two protonated and positively charged tertiary amines. Therefore, the protonation constants allow concluding that both H(**L**^{1})$^{3-}$ and H(**L**^{2})$^{2-}$ are present in the chair-chair conformation. Subsequent protonation steps occur on two carboxylates for **L**^{2}, while for **L**^{1}, logK_{H2} can be attributed to the phosphonate group and logK_{H3} and logK_{H4} correspond to carboxylate functions. The pyridine nitrogens are not protonated above pH 2. A previous, combined spectrophotometric and pH-metric study on **L**^{1} yielded similar protonation constants, with an additional value in the very acidic pH region which is not accessible in our potentiometric titration (logK_{Hi}: 11.5; 7.2; 3.8; 2.4; 0.5). In this study, the protonation scheme was also confirmed by ^{1}H- and ^{31}P pH-metric titrations.[21] We also note the higher basicity of the amine in the phosphonate than in the acetate derivative (logK_{H1}=11.51 for (**L**^{1})$^{4-}$ *vs*. 9.54 for (**L**^{2})$^{3-}$), in accordance with the usual trend observed for phosphonate-acetate substitutions which is explained by the increased positive inductive effect of the phosphonate. For instance, logK_{H1} increases from 11.9 for DOTA^{4-} to values between 12.6 and 14.65 for mono-, bis-, tris- and tetraphosphonate analogues of DOTA^{4-}.[40] A similar tendency was reported for the pyridine-containing macrocycles PC1A and PC1P (Scheme 1, Table 1)[32] and for other examples. [41-43]

Stability constants have been determined for Mn^{2+} and Zn^{2+} complexes (see Figure S3 for titration curves). The formation of the Mn^{2+} complex was found slow for [Mn(**L**^{2})]$^{-}$ (though faster than for [MnH**L**^{3}],[18] likely due to less steric crowding of the N7 substituent) requiring potentiometric measurements in batch samples. As an illustration, when mixing equimolar quantities of H(**L**^{2})$^{2-}$ and Mn^{2+} at pH 7.4 (50 mM HEPES, 25 °C) and following complex formation via relaxivity measurements, full complexation is achieved after ~30 mins. Complex formation was faster for [Mn(**L**^{1})]$^{2-}$ and did not exceed 10-15 mins in the pH range 2-7.

The stability constants for both Mn^{2+} and Zn^{2+} complexes are higher with the phosphonate than with the acetate analogue, mainly linked to the higher basicity of $(\mathbf{L^1})^{4-}$. This is generally observed for carboxylate *vs*. phosphonate derivatives, like in the case of Mn^{2+} and Zn^{2+} complexes formed with PC1A and PC1P (Table 1) or with DO2A ($\log K_{MnL}$ = 14.54)[44] and DO2P ($\log K_{MnL}$ = 18.10).[45] On the other hand, the conditional stabilities compared via the pM values (M = Mn, Zn) are rather close, with a slightly higher pM for the phosphonate derivative $H_2(\mathbf{L^1})^{2-}$. As expected, monoprotonated ($[M(H\mathbf{L^1})]^-$ and $[M(H\mathbf{L^2})]$) and diprotonated complexes ($[M(H_2\mathbf{L^1})]$) are also detected, in accordance with the presence of non-coordinating carboxylates on the bispidine skeleton and the possible protonation of the metal-coordinated phosphonate in $\mathbf{L^1}$. The comparison of the complex protonation constants for the complexes of $\mathbf{L^1}$ and $\mathbf{L^2}$ indicates that the first protonation step on $[Zn(\mathbf{L^1})]^{2-}$ and $[Mn(\mathbf{L^1})]^{2-}$ occurs on the phosphonate function, around pH 5.3, with a similar $\log K_H$ as for the PC1P analogues (Table 1). This is in perfect agreement with previous studies by variable-pH ^1H and ^{31}P NMR spectroscopy.[21] In line with the Irving-Williams series which predicts, for a given ligand, the lowest stability for Mn^{2+} among divalent first-raw transition metal ions, both $\mathbf{L^1}$ and $\mathbf{L^2}$ form more stable complexes with Zn^{2+} than with Mn^{2+}. For $[Zn(\mathbf{L^1})]^{2-}$, a higher absolute value was previously reported for the stability constant ($\log K_{ZnL}$ = 18.8)[21], which is mostly the consequence of considering an additional protonation constant in the acidic region (see above).

The species distribution curves calculated for 1 mM [Mn(**L**)] concentration by using the stability and protonation constants in Table 1 are represented in Figure 1. They indicate the presence of exclusively non-protonated complexes at physiological pH. These distribution curves are nicely corroborated by the pH-dependent relaxivities measured in aqueous solution of the two Mn^{2+} complexes, where the progressive relaxivity decrease follows the decreasing concentration of free Mn^{2+} upon complex formation. For $[Mn(\mathbf{L^2})]^-$, a slight inflection is visible in the relaxometric titration curve around pH 3.2 and can be attributed to the formation of the monoprotonated complex $[Mn(H\mathbf{L^2})]$.

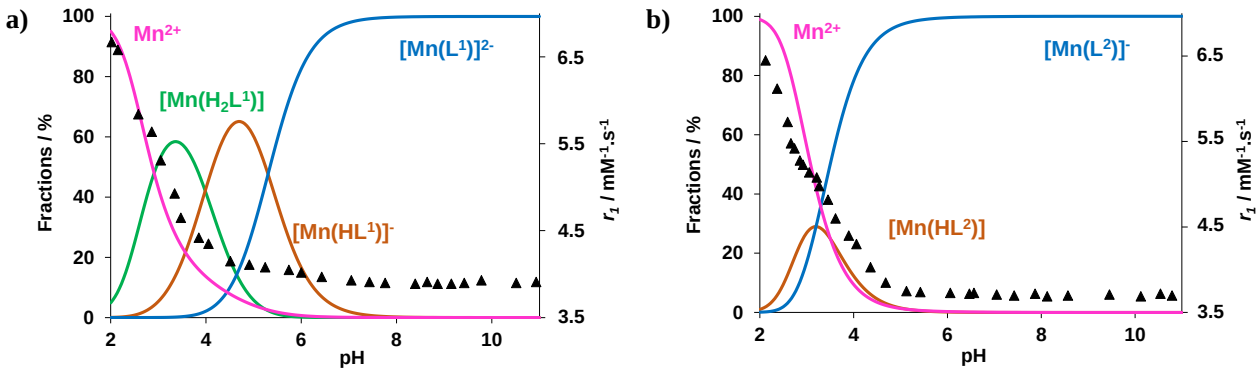

Figure 1. Species distribution curves calculated for $Mn^{2+}/\mathbf{L^1}$ (a) and $Mn^{2+}/\mathbf{L^2}$ (b) ($c_{Mn} = c_L = 1$ mM) and pH-dependent relaxivities (▲) measured at 25 °C, 60 MHz.

These thermodynamic stability constants and pM data indicate reasonable stabilities for $[Mn(\mathbf{L^1})]^{2-}$ and $[Mn(\mathbf{L^2})]^{-}$ species, nevertheless, they remain below the best values known for Mn^{2+} complexes. Indeed, the most stable macrocyclic complex with one inner-sphere water molecule $[Mn(PC2A\text{-}EA)]^{+}$ [15] (Scheme 1) has $\log K_{MnL} = 19.01$ and pM = 9.27, and an exceptionally high $\log K_{MnL} = 24.3$ and pM = 12.73 have been recently reported for the Mn^{2+} complex of a bispidine ligand containing five pyridine units which forms a peculiar, eight-coordinate structure with one water molecule in the first coordination sphere.[46]

Table 1. Ligand protonation constants, stability constants of ML complexes and pM values (I = 0.15 M NaCl ; 298 K). Values in parenthesis correspond to one standard deviation.

	$\mathbf{L^1}$	$\mathbf{L^2}$	$\mathbf{L^3}$ [18]	PC1A [25]	PC1P [25]
$\log K_{H1}$	11.15(1)	9.54(4)	11.44	10.47	11.84
$\log K_{H2}$	7.35(3)	5.11(6)	10.31	8.71	9.64
$\log K_{H3}$	3.78(4)	2.99(6)	4.71	2.79	6.23
$\log K_{H4}$	3.02(5)	-	2.76	-	0.99
$\log K_{H5}$	-	-	2.22	-	-
$\mathbf{\Sigma \log K_{Hi}}$	25.26	17.64	31.5	21.97	28.7
$\mathbf{\log K_{MnL}}$	13.72(3)	11.26(4)	12.21	11.54	14.06
$\log K_{MnHL}$	5.31(2)	3.20(3)	10.42	4.95	5.35
$\log K_{MnH2L}$	3.90(1)	-	3.87	-	-
$\mathbf{\log K_{ZnL}}$	16.54(4)	13.72(2)	15.59	17.01	19.66
$\log K_{ZnHL}$	5.43(3)	3.26(1)	10.33	3.03	5.19
$\log K_{ZnH2L}$	3.39(2)	-	3.28	-	-
pMn[a]	7.28	7.06	6.65	8.10	8.30

pZn[a]	8.76	8.29	8.40	-	-

[a] $c_M = c_L = 10^{-5}$ M ; pH 7.4.

Kinetic inertness

In general, Mn^{2+} complexes are known as particularly labile, though examples of higher inertness have been reported both with linear ligands (*trans*CDTA and derivatives)[47] and azamacrocycles (DOTA, PC2A derivatives).[15, 48] The rigidity of the ligand skeleton has been identified as an important structural element for the kinetic inertness of the complex. Recently, we have demonstrated unprecedented resistance to dissociation for the bispidine-derivative [Mn(H**L**^{3})] (Scheme 1), which is today by far the most inert Mn^{2+} chelate reported. Dissociation of metal complexes, including Mn^{2+} chelates, typically occurs *via* metal-assisted, proton-assisted and spontaneous pathways. The kinetic inertness can thus be assessed thus by the rate of transmetallation reactions in the presence of excess Zn^{2+} or Cu^{2+} or by the rate of dissociation in highly acidic conditions where the complex is thermodynamically not stable. For [Mn(**L**^{1})]$^{2-}$and [Mn(**L**^{2})]$^{-}$, we have followed Zn^{2+} transmetallation at varying pH by monitoring the variation of the proton relaxation rate (pH 3.1-6.0; with 50-fold Zn^{2+} excess to ensure pseudo-first order conditions, Figure 2). Although somewhat faster than for [Mn(H**L**^{3})], dissociation is extremely slow under these conditions. Complete transmetallation is not achieved even after 150 days at pH 5 for either of the two complexes, and at pH 6, the conversion amounts only to ~40% for [Mn(**L**^{1})]$^{2-}$ and ~20% for [Mn(**L**^{2})]$^{-}$ during the same time. The observed dissociation rate constants and the corresponding half-lives have been calculated for each pH (except pH 6 where the dissociation is too slow) and compared to analogous data for [Mn(H**L**^{3})] (Table 2). At pH 6 and in the presence of 25 equiv. of Zn^{2+}, the most inert macrocyclic chelates known reported so far have dissociation half-lives of 54.4 h ([Mn(PC2A-EA)]$^{+}$)[15] or 64.5 h ([Mn(PC2A-DPA)])[17], and the acyclic [Mn(PyC3A)]$^{-}$ has a half-life of 0.285 h.[14] The comparison with the $t_{1/2}$ of 138.5 h and 469.7 h determined at a lower pH = 5 for [Mn(**L**^{1})]$^{2-}$ and [Mn(**L**^{2})]$^{-}$, respectively, further illustrates the extraordinary kinetic inertness of our complexes. Transmetallation experiments have been also performed at varying Zn^{2+} concentrations for [Mn(**L**^{1})]$^{2-}$ and [Mn(H**L**^{3})] and showed very limited Zn^{2+} dependence (the maximum variation of k_{obs} was 3 % and 15% at pH 4.2 and 3.1, respectively, when varying the number of Zn^{2+}equivalents between 10 and 50).

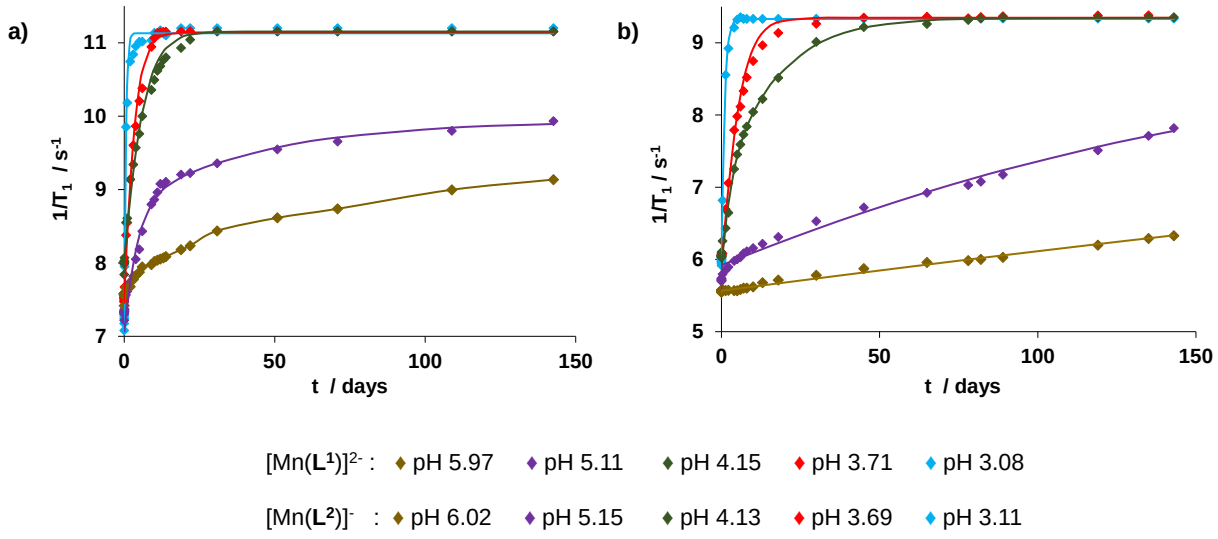

Figure 2. Time-dependent variation of the longitudinal proton relaxation rates in a 1.75 mM $[Mn(\mathbf{L}^1)]^{2-}$ (a) and 1.50 mM $[Mn(\mathbf{L}^2)]^{-}$ (b) solution at 37 °C and 60 MHz, 0.1 M NaCl, in the presence of 50 equiv. of Zn^{2+}. The curves represent the fit of the experimental data to yield the observed rate constants, k_{obs}.

Table 2. Observed pseudo-first order dissociation rate constants and corresponding half-lives calculated from data in Figure 2. T = 37 °C, I= 0.1 M NaCl.

Complexes	$k_{obs} \times 10^{-6}$ (s^{-1}) / $t_{1/2}$ **(pH 3.1)**	$k_{obs} \times 10^{-6}$ (s^{-1}) / $t_{1/2}$ **(pH 3.7)**	$k_{obs} \times 10^{-6}$ (s^{-1}) / $t_{1/2}$ **(pH 4.1)**	$k_{obs} \times 10^{-6}$ (s^{-1}) / $t_{1/2}$ **(pH 5.1)**
$[Mn(\mathbf{L}^1)]^{2-}$	24.93(5) / 7.72 h	4.37(2) / 1.84 d	2.64(2) / 3.04 d	1.39(1) / 5.77 d
$[Mn(\mathbf{L}^2)]^{-}$	14.33(4) / 13.44 h	2.90(2) / 2.77 d	1.79(2) / 4.48 d	0.41(3) / 19.57 d
$[Mn(H\mathbf{L}^3)]$[18]	8.47 / 22 h	0.82 / 10 d	0.24 / 33 d	0.06 / 137 d

For $[Mn(\mathbf{L}^1)]^{2-}$, the dissociation was also assessed in highly acidic solutions where it is much faster (0.01–1.0 M HCl, 25 °C; Figure 3), without Zn^{2+}. The observed rate constants show a second order dependence on the proton concentration, and could be fitted to Eq. 1 :

$$k_{obs} = k_0 + k_1[H^+] + k_2[H^+]^2 \quad \text{(Eq. 1)}$$

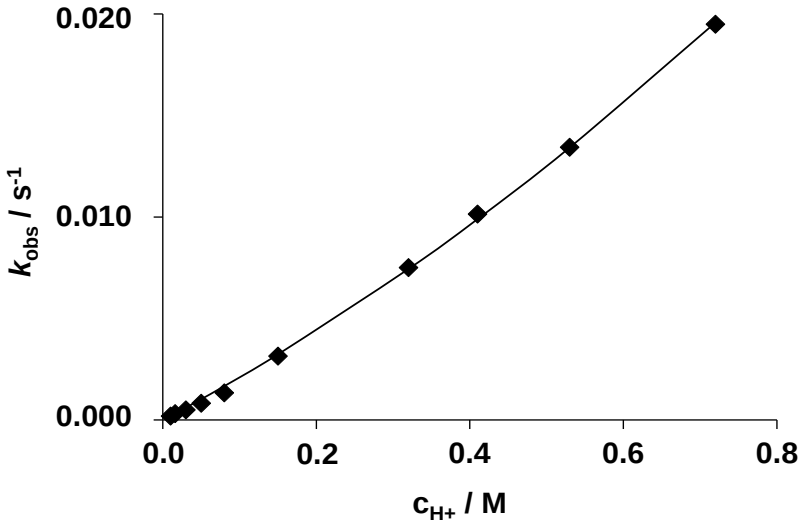

Figure 3 : Pseudo-first-order rate constants determined for the dissociation of $[Mn(\mathbf{L^1})]^{2-}$ in acidic solutions. The curve corresponds to the fit of the experimental data to Equation (1) as explained in the text. I = 1 M (HCl + NaCl), 25 °C.

The fit resulted in $k_1 = (20.1\pm0.5)\times10^{-3}$ $s^{-1}M^{-1}$ and $k_2 = (11\pm3)\times10^{-3}$ $s^{-1}M^{-2}$, while k_0 was fixed to 0, otherwise a negative value was obtained with a large error. The k_{obs} values determined above in the Zn^{2+} transmetalation study in the pH 3.1-5.1 interval also follow a second order dependence on $[H^+]$ for $[Mn(\mathbf{L^1})]^{2-}$ (Figure S4), with estimated values of $k_1 = (21.1\pm0.5)\times10^{-3}$ s^{-1} M^{-1} and $k_2 = (13\pm4)\times10^{-3}$ s^{-1} M^{-2}, very similar to the constants obtained from the study at higher acidity. For $[Mn(\mathbf{L^2})]^{-}$, the second order term is not visible in this acidity range (the k_{obs} *vs*. c_{H+} data define a straight line), thus only $k_1 = (17.9\pm0.5)\times10^{-3}$ s^{-1} M^{-1} can be calculated. The k_1 rate constant, characterizing the proton assisted dissociation pathway, is only ~15% higher for the phosphonate than for the acetate analogue. This similar inertness is quite remarkable, since the presence of phosphonate groups usually tends to be detrimental for kinetic inertness. For instance, the substitution of the acetate arm in HPC1A by a phosphonate (H_2PC1P) leads to the instantaneous dissociation of the Mn^{2+} complex at pH 6 in the presence of 5 equiv. of Zn^{2+}.[25] Likewise, the proton-assisted dissociation becomes seven orders of magnitude faster for $[Mn(DO3P)]^{4-}$ and for $[Mn(DOTP)]^{6-}$ [16, 25] than it is for $[Mn(DOTA)]^{2-}$ [49] (DOA3P = 1,4,7,10-tetraazacyclododecane-1,4,7-trisphosphonate-10-acetic acid ; DOTP = 1,4,7,10-tetraazacyclododecane-1,4,7,10-tetraphosphonate). The reason is that phosphonates can be protonated in slightly acidic solutions even when they are metal-bound, and this can facilitate proton transfer to the cyclen nitrogen, which is the rate-determining step in the dissociation of these tetraazamacrocyclic metal complexes. Interestingly, this detrimental effect is not observed in $[Mn(\mathbf{L^1})]^{2-}$, despite the possible protonation of the phosphonate group with a protonation constant very similar to those typically reported for phosphonate-derivative metal complexes. This important difference might indicate that in the dissociation of bispidine

complexes, the rate-determining step is different. One could speculate that the slowest, rate-determining step involves rather a structural reorganization of the bispidine scaffold than a proton transfer.

The observed dissociation rates (Table 2), as well as the calculated k_1 rate constants characterizing the proton-assisted dissociation are one order of magnitude higher for [Mn(H_2**L**^{1})] and [Mn(H**L**^{2})] than the corresponding values previously determined for [Mn(H_2**L**^{3})]$^{+}$ (k_1 = 1.6×10^{-3} s^{-1} M^{-1}; see Table 2 for the observed rates).[18] The tenfold higher inertness of [Mn(H**L**^{3})] might be the consequence of the increased steric crowding on the α carbon of the N7 substituent, although one cannot exclude that the pending lysine amine also plays a role by establishing strong hydrogen bonding with the non-coordinating carboxylates and further rigidifying the ligand structure. Despite this slight decrease in kinetic inertness with respect to [Mn(H**L**^{3})], both [Mn(**L**^{1})]$^{2-}$ and [Mn(**L**^{2})]$^{-}$ remain extremely resistant to dissociation and are among the most inert Mn^{2+} chelates described so far.

Relaxation properties

Proton relaxivities have been measured for [Mn(**L**^{1})]$^{2-}$ and [Mn(**L**^{2})]$^{-}$ at 25 and 37 °C, in water (pH 7) in the Larmor frequency range of 0.01-80 MHz (Figure. 4). The relaxivities amount to r_1 = 4.31 mM^{-1}s^{-1} and 3.67 mM^{-1}s^{-1} at 25 °C, 20 MHz, respectively, for [Mn(**L**^{1})]$^{2-}$ and [Mn(**L**^{2})]$^{-}$. They are comparable or slightly lower than r_1 = 4.28 mM^{-1}s^{-1} for [Mn(H**L**^{3})] [18] or r_1 = 4.74 mM^{-1}s^{-1} for the commercial MRI agent [Gd(DOTA)]$^{-}$,[19] but higher than relaxivities typically reported for Mn^{2+} complexes with q =1, such as [Mn(PCy3A)]$^{-}$ (3.3 mM^{-1}s^{-1})[14] or [Mn(PC2A-EA)]$^{+}$ (3.52 mM^{-1}s^{-1}),[15] in the same conditions. In order to gain more direct information on the hydration number and the water exchange parameters of the complexes, we have performed a variable temperature ^{17}O NMR study. By using the approach of Gale et al.,[50] the temperature-dependent ^{17}O transverse relaxation rates ($1/T_2$) allowed for the estimation of a hydration number of q = 0.96 for [Mn(**L**^{2})]$^{-}$, confirming monohydration (Figure S5). In the case of [Mn(**L**^{1})]$^{2-}$, this method is not applicable since no maximum is observed in the $1/T_2$ *vs*. temperature curve. However, based on the relaxivity values and on the analogy to [Mn(**L**^{2})]$^{-}$, we can reasonably estimate the inner-sphere hydration state to q =1 for [Mn(**L**^{1})]$^{2-}$.

We have analyzed the temperature-dependent transverse ^{17}O relaxation rates and the Proton Nuclear Magnetic Relaxation Dispersion (^{1}H NMRD) profiles of $[Mn(\mathbf{L^1})]^{2-}$ and $[Mn(\mathbf{L^2})]^{-}$ by using the common Solomon-Bloembergen-Morgan theory of paramagnetic relaxation and calculated the parameters describing water exchange and rotational dynamics (see ESI for details). In a previous report on $[Mn(H\mathbf{L^3})]$, we considered that the contribution from a second sphere relaxation mechanism, originating from water molecules hydrogen-bound to the non-coordinating carboxylates was important and explained the unexpectedly high relaxivity. The high relaxivity observed for $[Mn(\mathbf{L^1})]^{2-}$ suggests that a similar second sphere mechanism is operational to which the phosphonate group can also further contribute.[51] Therefore, for $[Mn(\mathbf{L^1})]^{2-}$ the ^{1}H NMRD profiles have been analyzed by assuming two 2nd sphere water molecules (with an estimated Mn-H proton distance of 3.2 Å, 50 ps residence time and an activation enthalpy of 10 kJ/mol, based on previous simulations on Gd^{3+} complexes). With a ~15 % lower relaxivity, the situation is less obvious for $[Mn(\mathbf{L^2})]^{-}$, despite the presence of the non-coordinating carboxylates. For this complex, we have carried out an analysis both with and without this second sphere contribution, which leads to slightly different values for the rotational correlation time, while all the other parameters remain essentially unchanged. In the fitting procedure, some parameters have been fixed to common values: the distance between the metal ion and the inner and outer sphere water protons (r_{MnH} = 2.83 Å and a_{MnH} = 3.6 Å, respectively); the diffusion coefficient and its activation energy ($D_{MnH} = 26\times10^{-10}$ m^2s^{-1} and E_{MnH} = 20 kJ mol^{-1}) and the activation energy for the modulation of the zero-field splitting

(E_v = 1 kJ mol^{-1}). The following parameters have been calculated and are shown in Table 3 : the rate (k_{ex}^{298}) and the activation enthalpy ($\Delta H^{\neq}$) and entropy ($\Delta S^{\neq}$) of the water exchange, the rotational correlation time (τ_{rH}^{298}) and its activation energy (E_{rH}), the ^{17}O scalar coupling constant ($A_o/\hbar$), and the parameters characterizing electron spin relaxation (τ_v^{298}) and (Δ^2). These parameters have been obtained considering the Solomon-Bloembergen-Morgan theory which uses a simplified description of the electronic relaxation taking into account only the fluctuations of the transient ZFS. Such theory is known to be less accurate at low field. A more accurate description of the electronic relaxation of these complexes would be obtained by considering also the contribution of the static ZFS which could be estimated from EPR measurements although such measurements are beyond the scope of the present study.[52]

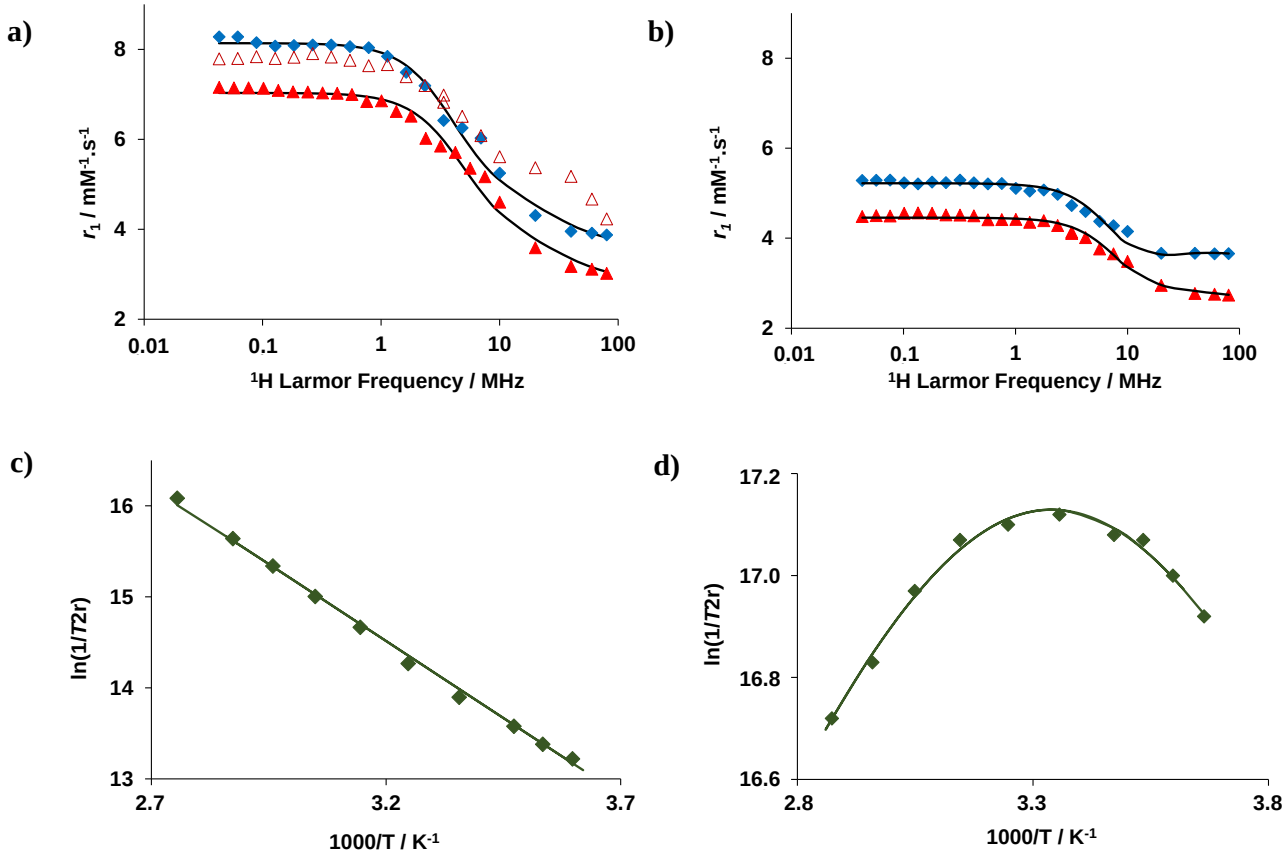

Figure 4 : Nuclear Magnetic Relaxation Dispersion profiles (NMRD) in water at 37 °C (▲) and 25 °C (♦) and human serum at 37 °C (Δ) for $[Mn(\mathbf{L}^1)]^{2-}$ (a) and $[Mn(\mathbf{L}^2)]^{-}$ (b) ; reduced transverse ^{17}O relaxation rates for $[Mn(\mathbf{L}^1)]^{2-}$ (c) and $[Mn(\mathbf{L}^2)]^{-}$ (d), 9.4 T. The lines represent the fit of the experimental points as explained in the text.

Table 3. Parameters obtained from the fit of ^{17}O NMR and ^{1}H NMRD data.

	$[Mn(\mathbf{L}^1)]^{2-}$	$[Mn(\mathbf{L}^2)]^{-}$	$[Mn(H\mathbf{L}^3)]$ [18]	[Mn(PC1P)] [25]	$[Mn(PC1A)]^{+}$ [25]
CN	6	6	6	6	6
q	1	1	1	1	1
r_1 /mM^{-1} .s^{-1} [a]	4.31	3.64	4.28	2.84	2.39
k_{ex}^{298} /10^7 s^{-1}	0.12(1)	5.5(1)	5.1	177	303
$\Delta H^{\neq}$ / kJ.mol^{-1}	25.7(7)	14.9(4)	10.6	14.0	13.0
$\Delta S^{\neq}$ / kJ.mol^{-1}	-42(2)	-47(1)	-62	-21	-20

E_{rH} / kJ.mol^{-1}	19(1)	20(1)	22	20.3	16.0
τ_{rH}^{298} / ps	92(2)[b]	89(2) 65(4)[b]	100 72[b]	38.6	23.0
τ_v^{298} / ps	22(1)	17(1)	24	14.3	8.7
Δ^2 /10^{19} s^{-2}	0.35(1)	1.64(9)	0.8	30.2	4.0
$A_o/\hbar$ /10^6 rad.s^{-2}	30.0(2)	33.2(2)	28	39.9	36.6

[a] 20 MHz and 25 °C. [b] considering a 2nd sphere relaxivity contribution.

The water exchange is considerably slower for the phosphonate derivative [Mn(**L**^{1})]$^{2-}$ than for the acetate analogues [Mn(**L**^{2})]$^{-}$ and [Mn(H**L**^{3})]. For all three complexes, the activation entropies calculated suggest a strong associative character of the mechanism, implying that the incoming water molecule enters the inner coordination sphere of the metal ion before the outgoing water leaves. Such associative mechanism can be indeed expected for these six-coordinate chelates, given the typical coordination numbers of 6 and 7 for Mn^{2+}. In an associative exchange process, both the increased negative charge and the bulkiness of the phosphonate derivative will restrict the arrival of the incoming water in the rate-determining step, thereby reducing the rate of the water exchange. Additionally, the coordinated water molecule can also establish stronger hydrogen bonds with a phosphonate group than with an acetate, which might also disfavor the exchange. Likewise, a decrease (though much more limited) in the water exchange rate was observed for phosphonate derivative [Mn(PC1P)] with respect to the acetate [Mn(PC1A)]$^{+25}$ (Table 3); these are also six-coordinate complexes with an associative exchange mechanism that was further confirmed by the negative activation volumes determined in a variable pressure ^{17}O NMR study.

The rotational correlation times obtained in the fits are reasonable for the size of the complexes. We should note, however, that the exact values should not be over-interpreted as they are strongly correlated with the magnitude of the second sphere relaxivity contribution considered in the analysis, which itself is very difficult to assess. In overall, one can reasonably state that the second sphere relaxation mechanism has a significant contribution to relaxivity at least for [Mn(**L**^{1})]$^{2-}$. In the presence of human serum, the relaxivities of [Mn(**L**^{1})]$^{2-}$ increase slightly (e.g. from 3.59 mM^{-1}s^{-1} in water to 5.37 mM^{-1}s^{-1} in serum at 37 °C; Figure 4.a), indicating low affinity binding to serum proteins. Relaxivity changes in the same order have been reported for [Mn(H**L**^{3})],[18] or for [Mn(PyC3A)]$^{-}$.[14]

$^{52}Mn^{2+}$ radiolabelling

We have produced and purified ^{52}Mn at the cyclotron of the Orléans CNRS campus, as previously reported.[18] The radiolabelling of $H_2(\mathbf{L^1})^{2-}$ was tested under different conditions of pH, temperature and ^{52}Mn:$\mathbf{L^1}$ ratio. The radiolabelling reactions were followed by radio TLC at different time points. All reactions were performed in presence of ascorbic acid to prevent any oxidation reaction. Optimized reaction conditions were obtained for pH 7, 15 min at room temperature, achieving > 99% labelling yield for a $1:10^4$ ^{52}Mn:$\mathbf{L^1}$ ratio. Lowering the ^{52}Mn:$\mathbf{L^1}$ ratio by 10-fold increased the labelling reaction time from 15 to 20 min which was fully achieved at 70 °C. The radiolabelling is faster than that observed for the bispidine analogue $\mathbf{L^3}$ for a similar ratio ($1:10^4$), the radiolabelling of $\mathbf{L^3}$ required the use of higher temperature and longer reaction times (1 h, 70 °C).[18]

$[^{52}Mn(\mathbf{L^1})]^{2-}$ is highly hydrophilic with a log*P* = -2.80±0.05, which falls within the range reported for other Mn complexes, e.g. $[^{52}Mn(H\mathbf{L^3})]$, $[Mn(DPDP)]^{4-}$ or $[Mn(EDTA\text{-}BTA)]^{2-}$ with log*P* values of -1.96, -3.07 and -1.84, respectively. As expected, $[Mn(\mathbf{L^1})]^{2-}$ is more hydrophilic than the previously studied $[^{52}Mn(H\mathbf{L^3})]$.

The *in vitro* stability of the radiocomplex was assessed in different media at pH 7.4 (water, PBS and saline (0.9% NaCl)) and in the presence of 0.6 mM HSA (Figure 5), revealing its stability in all media up to 24 h.

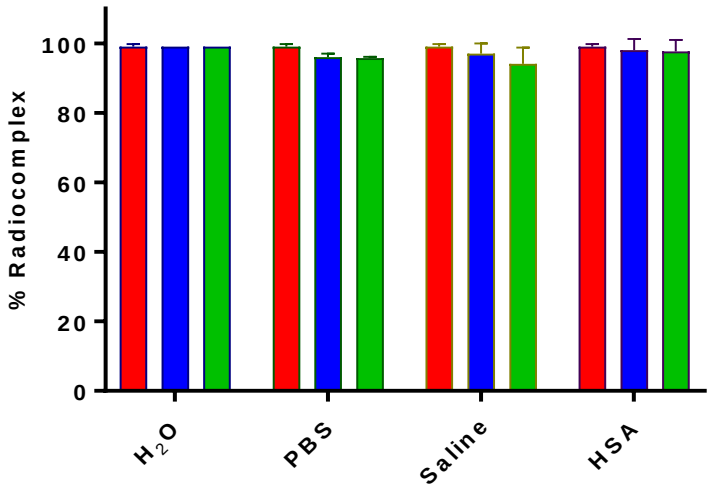

Figure 5: *In vitro* stability of $[^{52}Mn(\mathbf{L^1})]^{2-}$ in different media at pH 7.4 (water, PBS and saline (0.9% NaCl)) and in the presence of 0.6 mM HSA, at different time points : t_0 (red bars), 2h (blue bars) and 24 h (green bars).

Conclusion

Bispidine ligands bearing a phosphonate ($H_4\mathbf{L^1}$) or an acetate function ($H_3\mathbf{L^2}$) on the N7 position of the bicycle have been evaluated for the complexation of Mn^{2+} in the context of potential application as MRI contrast agents or ^{52}Mn PET tracers. Potentiometric data yielded ligand protonation constants and complex stability constants. A single protonation step is detected at basic pH, confirming chair-chair conformation for both ligands. Stability constants of Mn^{2+} and Zn^{2+} complexes follow the expected Irving-Williams order and correspond to similar and relatively moderate stabilities for $[Mn(\mathbf{L^1})]^{2-}$ and $[Mn(\mathbf{L^2})]^{-}$. Their dissociation kinetics has been assessed in Zn^{2+} transmetallation experiments between pH 3 and 6 and at higher acidity without Zn^{2+}, and shows extremely high kinetic inertness. At pH 6 and after 150 days, dissociation is limited to ~40% and ~20% for $[Mn(\mathbf{L^1})]^{2-}$ and $[Mn(\mathbf{L^2})]^{-}$, respectively, in the presence of 50 equiv. of Zn^{2+} (37 °C). Interestingly and in contrast to previous examples, the phosphonate complex is almost as inert as the acetate analogue, despite the potential protonation of the phosphonate group which previously was found to be responsible of an accelerated proton-catalyzed process.

The ^{1}H and ^{17}O relaxation properties are consistent with monohydration for both complexes. Interestingly, the water exchange rate is considerably lower for the phosphonate analogue, which might be the consequence of the higher negative charge and bulkiness of the phosphonate group which restricts the approach of the incoming water molecule in an associatively activated exchange process. Likely related to the contribution of a second sphere relaxation mechanism, the relaxivity of $[Mn(\mathbf{L^1})]^{2-}$ is remarkably high for a Mn^{2+} chelate with one inner-sphere water molecule. Finally, $\mathbf{L^1}$ could be successfully radiolabelled with ^{52}Mn and the radiocomplex has shown excellent stability for at least 24 hours in various biologically relevant media. Taken together, these features and in particular the excellent kinetic inertness of the complexes make these ligands highly interesting for Mn^{2+} chelation and confirm the great potential of Mn^{2+}-bispidines for the development of MRI and PET imaging agents.

ASSOCIATED CONTENT

Supporting Information. The following data are available free of charge. ^{1}H-^{1}H NOESY spectrum of compound 3 and its diastereoisomer (Figures S1-S2); potentiometric titration

curves for H_4L^1 and H_3L^2 (Figure S3); dependency of the k_{obs} values in Zn^{2+} transmetalation experiments for $[Mn(\mathbf{L^1})]^{2-}$ and $[Mn(\mathbf{L^2})]^{-}$ (Figure S4); ^{17}O transverse relaxivities of $[Mn(\mathbf{L^1})]^{2-}$ and $[Mn(\mathbf{L^2})]^{-}$ as a function of the temperature (Figure S5); ^{1}H NMR , ^{13}C NMR and ESI/MS spectra of compounds 1, 3 and H_3L^2 (Figure S6-S10); UV-vis spectra of $\mathbf{L^1}$ and $[Mn(\mathbf{L^1})]^{2-}$ (Figure S11). Analysis of ^{17}O NMR and ^{1}H NMRD data.

AUTHOR INFORMATION

Corresponding Author

*l.charbonn@unistra.fr; aline.nonat@unistra.fr, Equipe de Synthèse pour l'Analyse,

Université de Strasbourg, CNRS, IPHC UMR 7178, F-67 037 Strasbourg, France.

*eva.jakabtoth@cnrs-orleans.fr, Centre de Biophysique Moléculaire, CNRS UPR 4301,

Université d'Orléans, rue Charles Sadron, F-45071 Orléans, France.

Author Contributions

The manuscript was written through contributions of all authors. All authors have given approval to the final version of the manuscript. ‡These authors contributed equally.

Funding Sources

The authors thank the French Centre National de la Recherche Scientifique and the French National Research Agency (grant ANR-18-CE18-0008) for funding.

REFERENCES

(1) Grobner, T., Gadolinium - a specific trigger for the development of nephrogenic fibrosing dermopathy and nephrogenic systemic fibrosis. *Nephrol. Dial. Transplant.* **2006,** *21*, 1104-1108.
(2) Di Gregorio, E.; Ferrauto, G.; Furlan, C.; Lanzardo, S.; Nuzzi, R.; Gianolio, E.; Aime, S., The Issue of Gadolinium Retained in Tissues Insights on the Role of Metal Complex Stability by Comparing Metal Uptake in Murine Tissues Upon the Concomitant Administration of Lanthanum- and Gadolinium-Diethylentriamminopentaacetate. *Investig. Radiol.* **2018,** *53*, 167-172.
(3) Andreini, C.; Bertini, I.; Cavallaro, G.; Holliday, G. L.; Thornton, J. M., Metal ions in biological catalysis: from enzyme databases to general principles. *J. Biol. Inorg. Chem.* **2008,** *13*, 1205-1218.
(4) Arnold M, M. F., Stronach I, Pejovic-Milic A, Chettle D, Waker A, An accelerator based system for in vivo neutron activation analysis measurements of manganese in human hand bones. *Med. Phys* **2002,** *29*, 2718-24.

(5) Yingzi Liu 1, F. M., Daniel Sowers, Mindy Hsieh, Wei Zheng, Linda H Nie Customized Compact Neutron Activation Analysis System to Quantify Manganese (Mn) in Bone In Vivo. *Physiol. Meas.* **2017,** *38*, 452-465.
(6) Costa L, A. M., *Manganese in Health and Disease*. Royal Society of Chemistry: 2015; Vol. Chapter 14.
(7) Esteban-Gómez, D.; Cassino, C.; Botta, M.; Platas-Iglesias, C., 17O and 1H relaxometric and DFT study of hyperfine coupling constants in [Mn(H2O)6]2+. *RSC Adv.* **2014,** *4*, 7094-7103.
(8) Brandt, M.; Cardinale, J.; Rausch, I.; Mindt, T. L., Manganese in PET imaging: Opportunities and challenges. *J. Label. Compd. Radiopharm.* **2019,** *62*, 541-551.
(9) Saar, G.; Millo, C. M.; Szajek, L. P.; Bacon, J.; Herscovitch, P.; Koretsky, A. P., Anatomy, Functionality, and Neuronal Connectivity with Manganese Radiotracers for Positron Emission Tomography. *Molecular Imaging and Biology* **2018,** *20*, 562-574.
(10) Zhou, I. Y.; Ramsay, I. A.; Ay, I.; Pantazopoulos, P.; Rotile, N. J.; Wong, A.; Caravan, P.; Gale, E. M., Positron Emission Tomography–Magnetic Resonance Imaging Pharmacokinetics, In Vivo Biodistribution, and Whole-Body Elimination of Mn-PyC3A. *Investig. Radiol.* **2021,** *56*.
(11) Brücher, E.; Tircso, G.; Baranyai, Z.; Kovacs, Z.; Sherry, A. D., Stability and Toxicity of Contrast Agents. In *The Chemistry of Contrast Agents in Medical Magnetic Resonance Imaging*, Merbach, A. E.; Helm, L.; Toth, E., Eds. Wiley: New York: 2013; pp 157-208.
(12) Molnar, E.; Varadi, B.; Garda, Z.; Botar, R.; Kalman, F. K.; Toth, E.; Platas-Iglesias, C.; Toth, I.; Brucher, E.; Tircso, G., Remarkable differences and similarities between the isomeric Mn(II)-cis- and trans-1,2-diaminocyclohexane-N,N,N ',N '-tetraacetate complexes. *Inorganica Chim. Acta* **2018,** *472*, 254-263.
(13) Kalman, F. K.; Tircso, G., Kinetic Inertness of the Mn2+ Complexes Formed with AAZTA and Some Open-Chain EDTA Derivatives. *Inorg. Chem* **2012,** *51*, 10065-10067.
(14) Gale, E. M.; Atanasova, I. P.; Blasi, F.; Ay, I.; Caravan, P., A Manganese Alternative to Gadolinium for MRI Contrast. *J. Am. Chem. Soc.* **2015,** *137*, 15548-15557.
(15) Botár, R.; Molnár, E.; Trencsényi, G.; Kiss, J.; Kálmán, F. K.; Tircsó, G., Stable and Inert Mn(II)-Based and pH-Responsive Contrast Agents. *J. Am. Chem. Soc.* **2020,** *142*, 1662-1666.
(16) Garda, Z.; Molnar, E.; Kalman, F. K.; Botar, R.; Nagy, V.; Baranyai, Z.; Brucher, E.; Kovacs, Z.; Toth, I.; Tircso, G., Effect of the Nature of Donor Atoms on the Thermodynamic, Kinetic and Relaxation Properties of Mn(II) Complexes Formed With Some Trisubstituted 12-Membered Macrocyclic Ligands. *Front Chem* **2018,** *6*, 232.
(17) Botár, R.; Molnár, E.; Garda, Z.; Madarasi, E.; Trencsényi, G.; Kiss, J.; Kálmán, F. K.; Tircsó, G., Synthesis and characterization of a stable and inert MnII-based ZnII responsive MRI probe for molecular imaging of glucose stimulated zinc secretion (GSZS). *Inorg. Chem. Front.* **2022,** *9*, 577-583.
(18) Ndiaye, D.; Sy, M.; Pallier, A.; Même, S.; de Silva, I.; Lacerda, S.; Nonat, A. M.; Charbonnière, L. J.; Tóth, É., Unprecedented Kinetic Inertness for a Mn2+-Bispidine Chelate: A Novel Structural Entry for Mn2+-Based Imaging Agents. *Angew. Chem. Int. Ed.* **2020,** *59*, 11958-11963.
(19) Powell, D. H.; Dhubhghaill, O. M. N.; Pubanz, D.; Helm, L.; Lebedev, Y. S.; Schlaepfer, W.; Merbach, A. E., Structural and Dynamic Parameters Obtained from 17O NMR, EPR, and NMRD Studies of Monomeric and Dimeric Gd3+ Complexes of Interest in Magnetic Resonance Imaging: An Integrated and Theoretically Self-Consistent Approach1. *J. Am. Chem. Soc.* **1996,** *118*, 9333-9346.
(20) Drahoš, B.; Pniok, M.; Havlíčková, J.; Kotek, J.; Císařová, I.; Hermann, P.; Lukeš, I.; Tóth, É., Mn2+ complexes of 1-oxa-4,7-diazacyclononane based ligands with acetic, phosphonic and phosphinic acid pendant arms: Stability and relaxation studies. *Dalton Trans.* **2011,** *40*, 10131-10146.

(21) Gillet, R.; Roux, A.; Brandel, J.; Huclier-Markai, S.; Camerel, F.; Jeannin, O.; Nonat, A. M.; Charbonnière, L. J., A Bispidol Chelator with a Phosphonate Pendant Arm: Synthesis, Cu(II) Complexation, and 64Cu Labeling. *Inorg. Chem* **2017,** *56*, 11738-11752.
(22) Comba, P.; Jermilova, U.; Orvig, C.; Patrick, B. O.; Ramogida, C. F.; Rück, K.; Schneider, C.; Starke, M., Octadentate Picolinic Acid-Based Bispidine Ligand for Radiometal Ions. *Chem. Eur. J.* **2017,** *23*, 15945-15956.
(23) Kolanowski, J. L.; Jeanneau, E.; Steinhoff, R.; Hasserodt, J., Bispidine Platform Grants Full Control over Magnetic State of Ferrous Chelates in Water. *Chem. Eur. J.* **2013,** *19*, 8839-8849.
(24) Fulmer, G. R.; Miller, A. J. M.; Sherden, N. H.; Gottlieb, H. E.; Nudelman, A.; Stoltz, B. M.; Bercaw, J. E.; Goldberg, K. I., NMR Chemical Shifts of Trace Impurities: Common Laboratory Solvents, Organics, and Gases in Deuterated Solvents Relevant to the Organometallic Chemist. *Organometallics* **2010,** *29*, 2176-2179.
(25) Drahoš, B.; Kotek, J.; Císařová, I.; Hermann, P.; Helm, L.; Lukeš, I.; Tóth, É., Mn2+ Complexes with 12-Membered Pyridine Based Macrocycles Bearing Carboxylate or Phosphonate Pendant Arm: Crystallographic, Thermodynamic, Kinetic, Redox, and 1H/17O Relaxation Studies. *Inorg. Chem* **2011,** *50*, 12785-12801.
(26) Martell, A. E. M., *Determination and Use of Stability Constants*. Wiley-VCH: New York, 1992.
(27) P. Gans and B. O'Sullivan, G., *Protonic Softwares*. Leeds, U.K. and Berkeley, CA: 2005.
(28) Gans, P. G., a New Computer Program for Glass Electrode Calibration. *Talanta* **2000,** *1*, 33-37.
(29) Gans, P.; Sabatini, A.; Vacca, A., Investigation of equilibria in solution. Determination of equilibrium constants with the HYPERQUAD suite of programs. *Talanta* **1996,** *43*, 1739-1753.
(30) Raiford, D. S. F., C. L.; Becker, E. D, Calibration of Methanol and Ethylene Glycol Nuclear Magnetic Resonance Thermometers. *Anal. Chem* **1979,** *12*, 2050-51.
(31) Hugi, A. D. H., L.; Merbach, A. E, Water Exchange on Hexaaquavanadium(III): a Variable-Temperature and Variable-Pressure17O-NMR Study at 1.4 and 4.7 Tesla. *Helv. Chim. Acta* **1985,** *2*, 508-521.
(32) Drahoš, B.; Kotek, J.; Hermann, P.; Lukeš, I.; Tóth, É., Mn2+ Complexes with Pyridine-Containing 15-Membered Macrocycles: Thermodynamic, Kinetic, Crystallographic, and 1H/17O Relaxation Studies. *Inorg. Chem* **2010,** *49*, 3224-3238.
(33) Meiboom, S. G., D, Modified Spin- Echo Method for Measuring Nuclear Relaxation Times. *Rev. Sci. Instrum.* **1958,** *8*, 688-91.
(34) Micskei, K.; Helm, L.; Brucher, E.; Merbach, A. E., Oxygen-17 NMR study of water exchange on gadolinium polyaminopolyacetates [Gd(DTPA)(H2O)]2- and [Gd(DOTA)(H2O)]- related to NMR imaging. *Inorg. Chem* **1993,** *32*, 3844-3850.
(35) Tóth, E.; Helm, L.; Merbach, A. E., Relaxivity of Gadolinium(III) Complexes: Theory and Mechanism. In *The Chemistry of Contrast Agents in Medical Magnetic Resonance Imaging*, 2013; pp 25-81.
(36) Legdali, T.; Roux, A.; Platas-Iglesias, C.; Camerel, F.; Nonat, A. M.; Charbonnière, L. J., Substitution-Assisted Stereochemical Control of Bispidone-Based Ligands. *J. Org. Chem.* **2012,** *77*, 11167-11176.
(37) Roux, A.; Nonat, A. M.; Brandel, J.; Hubscher-Bruder, V.; Charbonnière, L. J., Kinetically Inert Bispidol-Based Cu(II) Chelate for Potential Application to 64/67Cu Nuclear Medicine and Diagnosis. *Inorg. Chem* **2015,** *54*, 4431-4444.
(38) Norrehed, S.; Erdélyi, M.; Light, M. E.; Gogoll, A., Protonation-triggered conformational modulation of an N,N′-dialkylbispidine: first observation of the elusive boat–boat conformer. *Org. Biomol. Chem* **2013,** *11*, 6292-6299.

(39) Nonat, A. M.; Roux, A.; Sy, M.; Charbonnière, L. J., 2,4-Substituted bispidines as rigid hosts for versatile applications: from κ-opioid receptor to metal coordination. *Dalton Trans.* **2019,** *48*, 16476-16492.
(40) Campello, M. P. C.; Lacerda, S.; Santos, I. C.; Pereira, G. A.; Geraldes, C. F. G. C.; Kotek, J.; Hermann, P.; Vaněk, J.; Lubal, P.; Kubíček , V.; Tóth, É.; Santos, I., Lanthanide(III) Complexes of 4,10-Bis(phosphonomethyl)-1,4,7,10-tetraazacyclododecane-1,7-diacetic acid (trans-H6do2a2p) in Solution and in the Solid State: Structural Studies Along the Series. *Chem. Eur. J.* **2010,** *16*, 8446-8465.
(41) Abada, S.; Lecointre, A.; Elhabiri, M.; Esteban-Gómez, D.; Platas-Iglesias, C.; Tallec, G.; Mazzanti, M.; Charbonnière, L. J., Highly relaxing gadolinium based MRI contrast agents responsive to Mg2+ sensing. *Chem. Comm.* **2012,** *48*, 4085-4087.
(42) Abada, S.; Lecointre, A.; Elhabiri, M.; Charbonnière, L. J., Formation of very stable and selective Cu(ii) complexes with a non-macrocyclic ligand: can basicity rival pre-organization? *Dalton Trans.* **2010,** *39*, 9055-9062.
(43) Brandel, J.; Lecointre, A.; Kollek, J.; Michel, S.; Hubscher-Bruder, V.; Déchamps-Olivier, I.; Platas-Iglesias, C.; Charbonnière, L. J., Tetraphosphonated thiophene ligand: mixing the soft and the hard. *Dalton Trans.* **2014,** *43*, 9070-9080.
(44) Garda, Z.; Forgács, A.; Do, Q. N.; Kálmán, F. K.; Timári, S.; Baranyai, Z.; Tei, L.; Tóth, I.; Kovács, Z.; Tircsó, G., Physico-chemical properties of MnII complexes formed with cis- and trans-DO2A: thermodynamic, electrochemical and kinetic studies. *J. Inorg. Biochem.* **2016,** *163*, 206-213.
(45) Burai, L.; Ren, J.; Kovacs, Z.; Brücher, E.; Sherry, A. D., Synthesis, Potentiometry, and NMR Studies of Two New 1,7-Disubstituted Tetraazacyclododecanes and Their Complexes Formed with Lanthanide, Alkaline Earth Metal, Mn2+, and Zn2+ Ions. *Inorg. Chem* **1998,** *37*, 69-75.
(46) Cieslik, P.; Comba, P.; Dittmar, B.; Ndiaye, D.; Tóth, É.; Velmurugan, G.; Wadepohl, H., Exceptional Manganese(II) Stability and Manganese(II)/Zinc(II) Selectivity with Rigid Polydentate Ligands**. *Angew. Chem. Int. Ed.* **2022,** *61*, e202115580.
(47) Molnár, E.; Váradi, B.; Garda, Z.; Botár, R.; Kálmán, F. K.; Tóth, É.; Platas-Iglesias, C.; Tóth, I.; Brücher, E.; Tircsó, G., Remarkable differences and similarities between the isomeric Mn(II)-cis- and trans-1,2-diaminocyclohexane-N,N,N′,N′-tetraacetate complexes. *Inorganica Chim. Acta* **2018,** *472*, 254-263.
(48) Bianchi, A.; Calabi, L.; Giorgi, C.; Losi, P.; Mariani, P.; Palano, D.; Paoli, P.; Rossi, P.; Valtancoli, B., Thermodynamic and structural aspects of manganese(II) complexes with polyaminopolycarboxylic ligands based upon 1,4,7,10-tetraazacyclododecane (cyclen). Crystal structure of dimeric [MnL]2·2CH3OH containing the new ligand 1,4,7,10-tetraazacyclododecane-1,4-diacetate. *J. Chem. Soc., Dalton trans.* **2001**, 917-922.
(49) Drahoš, B.; Kubíček, V.; Bonnet, C. S.; Hermann, P.; Lukeš, I.; Tóth, É., Dissociation kinetics of Mn2+ complexes of NOTA and DOTA. *Dalton Trans.* **2011,** *40*, 1945-1951.
(50) Gale, E. M.; Zhu, J.; Caravan, P., Direct Measurement of the Mn(II) Hydration State in Metal Complexes and Metalloproteins through O-17 NMR Line Widths. *J. Am. Chem. Soc.* **2013,** *135*, 18600-18608.
(51) Elhabiri, M.; Abada, S.; Sy, M.; Nonat, A.; Choquet, P.; Esteban-Gómez, D.; Cassino, C.; Platas-Iglesias, C.; Botta, M.; Charbonnière, L. J., Importance of Outer-Sphere and Aggregation Phenomena in the Relaxation Properties of Phosphonated Gadolinium Complexes with Potential Applications as MRI Contrast Agents. *Chem. Eur. J.* **2015,** *21*, 6535-6546.
(52) Belorizky, E.; Fries, P. H.; Helm, L.; Kowalewski, J.; Kruk, D.; Sharp, R. R.; Westlund, P.-O., Comparison of different methods for calculating the paramagnetic relaxation enhancement of nuclear spins as a function of the magnetic field. *The Journal of Chemical Physics* **2008,** *128*, 052315.

SYNOPSIS

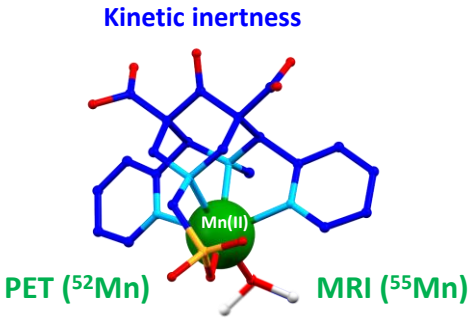

52/55-maganese complexes with ligand L^1, a bispidine-type ligand bearing a phosphonate substituent, possess a great potential for the development of MRI and PET imaging agents with remarkable relaxivity, extremely high kinetic inertness, quasi-quantitative radiolabelling and good stability in biological media.